RSC Advances

PAPER

Cite this: *RSC Adv.*, 2020, **10**, 3659

Study of ^{223}Ra uptake mechanism on hydroxyapatite and titanium dioxide nanoparticles as a function of pH

Petra Suchánková, Ekaterina Kukleva, Karel Štamberg, Pavel Nykl, Martin Vlk and Ján Kozempel *

Received 30th October 2019
Accepted 14th January 2020

DOI: 10.1039/c9ra08953e

rsc.li/rsc-advances

The mechanism of ^{223}Ra uptake on hydroxyapatite and titanium dioxide nanoparticles was studied as a function of pH. Both materials are widely used in food industry and medicine. They offer properties suitable for labelling with medicinal radionuclides, particularly for targeted radionuclide therapy. The selected isotope, ^{223}Ra, is an alpha emitter widely used in targeted alpha particle therapy due to high-dose delivery in very small tissue volume, nevertheless the results are applicable for any radium isotope including ^{226}Ra. The study was performed in the pH range 4.5 to 12 for hydroxyapatite nanoparticles and 2 to 12 for titanium dioxide nanoparticles in Britton–Robinson buffer solution. Both nanomaterials at pH 6 and higher showed that over 95% of the radium has been sorbed. According to the applied chemical equilibrium model, the most important species playing a role in sorption on the edge-sites were $RaCO_3$, $RaPO_4^-$, $RaHPO_4$ and $Ra(Ac^-)_2$, and Ra^{2+} and $RaH_2PO_4^+$ on layer-sites. All experiments were conducted under free air conditions and no negative impact of CO_2 was found. The surface complexation model was found suitable for describing radium uptake by the studied hydroxyapatite and titanium dioxide nanomaterials.

Introduction

Hydroxyapatite (HAp) and titanium dioxide are materials intensely studied and widely used for their favorable properties in many fields. Due to this, the range of their applications is extended from foodstuffs, cosmetics and sunscreen creams through environmental decontamination to medicine, which is our area of interest. Both materials are biocompatible and have relatively low clinical toxicity (LD_{50}, HAp (oral, rat) over 25 g kg^{-1}; LD_{50}, TiO_2 (oral, rat) over 10 g kg^{-1}), which is the underlying assumption for using them for patient applications.[1] Some advantages of radionuclide sorption are the following properties: high specific surface area, radiation stability and size. Apart from the previously mentioned reasons, ease of synthesis on a nanoscale size is another argument for selection of these two materials.[2–7]

Our main area of interest is specifically the possibility of the application of the chosen nanomaterials as a drug carrier system for diagnostic, therapeutic or theragnostic radionuclides. The targeting of the nanoparticles to the required tissue can be enabled by two mechanisms. The first one is passive targeting due to the Enhanced Permeability and Retention effect (EPR effect). This effect exploits the size of the drug carriers. Tumor tissue grows fast and stimulates angiogenesis. Conveniently, the novel blood vessels are abnormal and leaky, so the nanocarriers can get stuck in the tumor tissue.[8–10] The second one is active targeting by functionalization of the drug carrier surface. The carriers can be modified by specific ligands or antigens and the drugs are delivered to the target tissue due to their bond to the required receptor.[11] The basic principles of nanocarriers' preparation for the targeted alpha particle therapy (TAT), particularly bearing the alpha-emitting nuclides that decay in series, were described previously.[12]

Accordingly, hydroxyapatite (*n*HAp) and titanium dioxide nanoparticles (nTiO$_2$) could be applied as useful vehicles for radionuclide delivery in case of radiolabelling with an appropriate radionuclide, such as ^{18}F, ^{68}Ga, ^{99m}Tc *etc.* for diagnostic purposes or ^{225}Ac, ^{213}Bi, ^{177}Lu, ^{223}Ra, ^{186}Re, ^{90}Y and others for therapeutic purposes.[13–20] Nowadays, there are several publications dealing with radiolabelling of *n*HAp and nTiO$_2$. For example, there are published studies, where the *n*HAp is labelled by alpha therapeutic radionuclide – ^{223}Ra.[12] Other radionuclides used for labelling were ^{134,137}Cs or ^{90}Sr, where the *n*HAp was applied for remediation of contaminated waters by anthropogenic radionuclides.[21] Available published data for radiolabelling of nTiO$_2$ are limited. There are some studies dedicated to labelling of TiO_2 with ^{48}V or ^{125}I for *in vivo* toxicological studies[22,23] and with ^{225}Ac for targeted alpha radionuclide therapy.[24]

This article is focused on the study of ^{223}Ra sorption on *n*HAp and nTiO$_2$. The published data on radium sorption using

Czech Technical University in Prague, Faculty of Nuclear Sciences and Physical Engineering, Department of Nuclear Chemistry, Břehová 7, 11519 Prague 1, Czech Republic. E-mail: jan.kozempel@fjfi.cvut.cz

chosen nanoparticles are quite limited and available papers are focused mainly on ^{226}Ra behavior in uranium mill tailings and the articles studied only iron compounds as a goethite or ferrihydrite, or environmental minerals.[25–27]

The ^{223}Ra is a radionuclide used for TAT as radium chloride (Xofigo®).[12,28–30] Due to the cascade of emitted alpha particles, it could provide accurate high-dose irradiation of the target tissue (range of the alpha particles approx. 10 cells) without damage to the organism, if appropriate targeting strategy is applied. Nowadays, Xofigo® is used for the therapy of metastatic prostate cancer, but number of its applications decreases. Possible fields and ways of its applications could be significantly wider due to the capture of recoil nuclei by the nanoparticles and advantages of ^{223}Ra. Furthermore, ^{223}Ra can be obtained from a radionuclide generator ^{227}Ac/^{227}Th/^{223}Ra,[28–33] which can probably guarantee availability of the radionuclide in the hospitals. Main introduced disadvantage of ^{223}Ra are recoil nuclei appearing during the radioactive decay. They have considerable energy, which means, that daughter nuclei are escaping from chemical bonds and are distributed into the organism due to their chemical and biological properties. In the case of ^{223}Ra (α-emitter, $T_{1/2} = 11.4$ days), its daughter decay products with half-lives longer than one minute are: ^{211}Pb (β^--emitter, $T_{1/2} = 36.1$ min), ^{211}Bi (α-emitter, $T_{1/2} = 2.1$ min) and ^{207}Tl (β^--emitter, $T_{1/2} = 4.8$ min).[34]

The aim of this work is focused on the study of ^{223}Ra sorption as a function of pH. The mechanism of radium uptake by *n*HAp and *n*TiO_2 in Britton–Robinson buffer solution (BRB) was modelled and absorbed species were studied. For describing the surface complexation systems, chemical equilibrium model (CEM) was used. Modelling programs and codes for study of sorption mechanism requires protonation constants, ion-exchange constants and total concentration of edge-sites and layer-sites, which were determined experimentally *via* titration method and corresponding models.[35–37]

Experimental

Materials

All chemicals were of analytical grade purchased from Merck Millipore (Germany) and were used without further purification: sodium hydroxide, tetrabutyl *ortho*-titanate (TBOT), 2-propanol (IPA), ammonium hydroxide, phosphoric acid, nitric acid, methanol, boric acid, acetic acid, calcium nitrate tetrahydrate and diammonium hydrogen phosphate. Demineralized water of 18 MΩ cm^{-1} was obtained from water purification system (Millipore, USA). The activities of the samples were measured with a well-type NaI(Tl) crystal detector (Capintec, USA). For mixing of samples, Stuart SSM3 rocker (Cole-Parmer Ltd, United Kingdom) was used and the separation was made on VWR Micro Star 12 centrifuge (VWR International, LLC, USA). Gamma spectra were recorded on Canberra Packard HPGe detector (USA) under GammaVision software.

Britton–Robinson buffer solution

For Britton–Robinson buffer solution preparation in the pH ranging from 2 to 12, two stock solutions were mixed in appropriate ratio. The first one was 0.2 M sodium hydroxide and the second one was the mixture of 0.04 M phosphoric acid, 0.04 M boric acid and 0.04 M acetic acid.

Preparation of ^{223}Ra stock solution

The ^{223}Ra was eluted from ^{227}Ac/^{227}Th/^{223}Ra generator, which was prepared at our laboratory based on the study published by Guseva *et al.*[33] The column of the generator was filled with 0.5 g of Dowex-1 × 8 and ^{227}Ac in equilibrium with its decay products was loaded on it. The elution was provided by 0.7 M nitric acid in 80% methanol solution for the separation of ^{223}Ra from ^{227}Ac and ^{227}Th. The eluted ^{223}Ra$(NO_3)_2$ solutions were dried and reconstituted with deionized water. Possible breakthrough of parent radionuclides was checked by gamma spectrometry and was not observed in the eluate.

Sorbent materials preparation

The sorbent preparation was described by Kukleva *et al.* in detail.[35] In this article only brief procedure is mentioned.

For hydroxyapatite nanoparticles preparation, 1.2 M $Ca(NO_3)_2$ (24 mL) was added into 0.5 L of demineralized water. It was necessary to set and maintain the pH of the mixture to 11 with ammonium hydroxide. Afterwards, the solution of calcium nitrate was stirred and 0.7 M $(NH_4)_2HPO_4$ (24 mL) was added dropwise. The mixture was left overnight under stirring, washed three times with demineralized water (20 mL) and then dried under vacuum.

The titanium dioxide nanoparticles were prepared by the dropwise addition of the mixture of TBOT (1 mL) in IPA (4 mL) into demineralized water in ultrasonic generator and was stirred for 30 minutes. Prepared *n*TiO_2 were washed three times with demineralized water (20 mL), once with IPA (10 mL) and then dried under vacuum.

Sorption experiments

Experiments were performed in pH range from 4.5 to 12 for *n*HAp and from 2 to 12 for *n*TiO_2. All samples were in triplets and were prepared in a following way: 2 mg of *n*HAp or 5 mg of *n*TiO_2 were dispersed in 1 mL of BRB. Then 50 μL of ^{223}Ra$(NO_3)_2$ was dosed into each sample vial (pH of Ra solution was adjusted before adding to the sample by diluted ammonium hydroxide to the approx. sample pH in order not to exceed BRB's buffering capacity). Added radioactivity was ranged between 1.4 and 2.4 kBq. All samples were shaken for 24 hours, centrifuged and the supernatant was quantitatively removed. Then samples were dispersed in 1 mL of demineralized water in order to ensure same geometry of measurement. All samples and all supernatants were measured. All experiments were accomplished under free air conditions and at the laboratory temperature.

In the same manner, sorption of pure ^{223}Ra (without addition of nanomaterials) on the vial walls was studied in pH range from 2 to 12.

Modelling of the ^{223}Ra uptake

First of all, calculations of ^{223}Ra speciation diagrams were performed based on stability constants of Ra^{2+} mainly. In the

case of unavailable Ra constants, Ba^{2+}, Sr^{2+} and Ca^{2+} were used and were chosen due to their similar chemical properties. The stability constant values were taken from the Hatches database used in the geochemical code PhreeqC.[38]

Then the model based on the surface complexation theory was constructed and incorporated into the simulation code. According to the surface complexation theory, it is supposed that there are two types of surface functional groups: edge-sites and layer-sites. Their concentrations were already calculated based on experimental data.[35,36] For further modelling protonation constants of edge-sites, ion-exchange constant of layer-sites and the total concentration of both sites were used as input data.

The software product FAMULUS[39] and our code Praspec6.fm (code package STAMB 2017) were used for the speciation calculations. The corresponding code, Pramg6ZM.fm (code package STAMB 2017), is based on the Newton–Raphson multidimensional nonlinear regression used for experimental data fitting. It has to be added, that the number of complexing reactions, which can be used in calculation, is selectable. The appropriateness of the fit is evaluated by the χ^2-test, and the values of χ^2 are used to the calculation of criterion WSOS/DF (weighted sum of squares divided by degrees of freedom).[40] It holds, if $0.1 < WSOS/DF < 20$, then there is a good agreement between the experimental and the calculated data.

Results and discussion

As mentioned above, published studies[25–27] were focused only on ^{226}Ra and the sorption was studied only on a few materials.

Table 1 Comparison of stability constants (β) and solubility products (SP) of Ra and Ca complexes[38,41]

	log β/log SP	
Compound	Ra^{2+}	Ca^{2+}
CO_3^{2-}	2.50/−8.30	3.15/−8.14
Cl^-	−0.10	−0.29
SO_4^{2-}	2.75	2.31
OH^-	−13.49	−12.78

For the medicinal purposes, the attention was paid to the sorption of ^{223}Ra in BRB and it was experimentally studied on *n*HAp in the pH range of 4.5–12 and of 2–12 for $nTiO_2$. Studied pH ranges were different due to dissolution of the HAp under pH 4.5 while TiO_2 is stable in a wide pH range. The BRB consists of sodium compounds derived from phosphoric, boric and acetic acids – the speciation of which strongly depends on the pH value. Not only the corresponding ^{223}Ra complexes have to be taken into account, but also the hydroxo- and carbonate-complexes especially if the pH is higher than 7 due to dissolution of atmospheric CO_2.

Sorption of ^{223}Ra on superparamagnetic iron oxide nanoparticles (nFe_3O_4, SPIONs) was studied earlier in our laboratory,[42] therefore, in the current work the results of ^{223}Ra sorption on *n*HAp and $nTiO_2$ were compared with SPIONs.

Calculation of speciation diagram for ^{223}Ra in Britton–Robinson buffer solution

At first, it was necessary to draw attention to the fact, that the present state of stability constants knowledge for radium complexes was limited. The reliable values of studied complexes were available only for $RaOH^+$ and $RaCO_3$. Therefore, stability constants were taken into consideration for elements with similar chemical properties, namely for Ba, Sr and Ca. Unfortunately, data availability for Ba was also not sufficient, for Sr it was slightly better, but constants for acetic and boric acids complexes were also not available. Therefore, stability constants for Ca with above mentioned ligands were taken in addition to Ra hydroxo- and carbonate-complexes constants. The similarity of Ra and Ca complexation is demonstrated in Table 1 on the values of stability constants (β) and solubility product (SP)[38,41] (the values hold for $I = 0$).

The calculation of speciation diagrams were performed for the following composition of aqueous phase: 5.00×10^{-12} mol L^{-1} $Ra(NO_3)_2$; $\sum[H_3PO_4] = 4.00 \times 10^{-2}$ mol L^{-1}; $\sum[H_3BO_3] = 4.00 \times 10^{-2}$ mol L^{-1}; $\sum[CH_3COOH] = 4.00 \times 10^{-2}$ mol L^{-1}; $pCO_2 = 3.16 \times 10^{-4}$ at, ionic strength I ≈ 0.15. It deals with sodium salts of above-mentioned acids in a case of higher pH values.

The values of stability and dissociation constants ($I = 0$) are summarized in Table 2 and the results of calculation are shown

Table 2 The values of stability and dissociation constants ($I = 0$)[38,41]

Ligand	Stability constant	log *K*	Dissociation constant	log *K*
$H_2PO_4^-$	$K = [CaH_2PO_4]/([Ca]\cdot[H_2PO_4])$	1.28	$K = [HPO_4]/([H]\cdot[PO_4])$	12.36
HPO_4^{2-}	$K = [CaHPO_4]/([Ca]\cdot[HPO_4])$	2.68	$K = [H_2PO_4]/([H]^2\cdot[PO_4])$	19.70
PO_4^{3-}	$K = [CaPO_4]/([Ca]\cdot[PO_4])$	6.46	$K = [H_3PO_4]/([H]^3\cdot PO_4])$	21.93
$H_2BO_3^-$	$K = [CaH_2BO_3^+]/([Ca]\cdot[H_2BO_3^-])$	1.80	$K = [HCO_3]/([H]\cdot[CO_3])$	10.33
OH^-	$K = [RaOH]/([Ra]\cdot[OH])$	−0.5	$K = [H_2CO_3]/([H]^2\cdot[CO_3])$	16.68
CO_3^{2-}	$K = [RaCO_3]/([Ra]\cdot[CO_3])$	2.50	$K_p = [pCO_2]/([H]^2\cdot[CO_3])$	18.60[a]
Ac^-	$K = [CaAc^+]/[Ca^{2+}]\cdot[Ac^-]$	1.18	$K = [HAc]/([H]\cdot[Ac])$	4.76
$(Ac^-)_2$	$K = [Ca(Ac)_2]/[Ca^{2+}]\cdot[(Ac^-)_2]$	4.00	$K=([H_2BO_3]\cdot[H])/[H_3BO_3]$	−9.24
$(Ac^-)_3$	$K = [Ca(Ac)_3^-]/[Ca^{2+}]\cdot[(Ac^-)_3]$	4.45	$K=([HBO_3]\cdot[H])/[H_2BO_3]$	−12.74
$(Ac^-)_4$	$K = [Ca(Ac)_4^{2-}]/[Ca^{2+}]\cdot[(Ac^-)_4]$	3.60	$K=([BO_3]\cdot[H])/[HBO_3]$	−13.79
—	$SP = [Ra]\cdot[CO_3]$	−8.30	$K_v = [H]\cdot[OH]$	−14

[a] pCO_2 [at] – partial pressure of CO_2, atmospheric $pCO_2 = 3.16 \times 10^{-4}$ [at], $Ac = CH_3COO^-$.

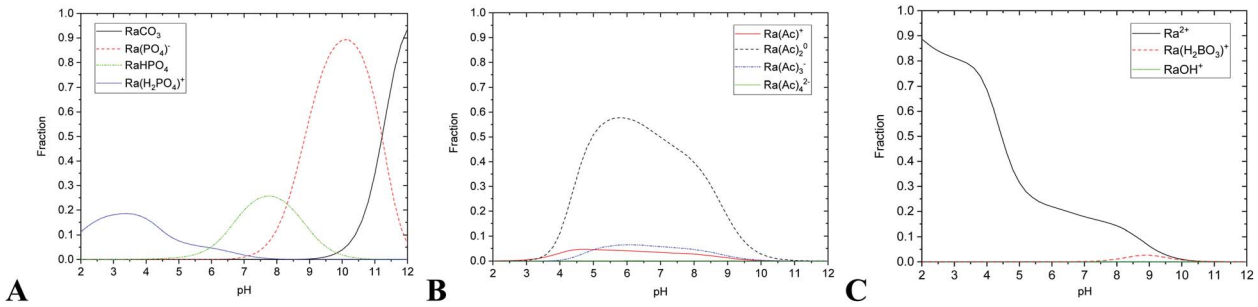

Fig. 1 The relative abundances of studied radium species on pH (A) phosphate and carbonate complexes, (B) acetate complexes, (C) ionic radium, hydroxyl and borate complex; total $\sum_{\text{Ra species}} = 1$.

in Fig. 1. Complexing reactions and corresponding complex compounds were incorporated in the code Praspec6.fm (Table 2.). Under the given conditions, only five of them can be regarded as more important, namely, the complexing reactions with PO_4^{3-}, HPO_4^{2-},$H_2PO_4^-$, CO_3^{2-} and $(CH_3COO^-)_2$. The calculation of possible precipitation of $RaCO_3$ was also considered in code Praspec6.fm, however, due to the very low Ra concentration, precipitation could not occur.

Modelling of experimental data as a function of pH

Chemical equilibrium model[36] was used to describe the surface complexation systems. It consisted of two groups of equations. The first one characterized the protonation and ion-exchange behavior of sites (eqn (1)–(3)) and the second one the sorption of individual species including the balance equations (eqn (4)–(12)). The values of sorption constants, K, (eqn (4)–(10)) were obtained during iterations.

The equations (eqn (1)–(12)) listed below were incorporated in the regression function of the code Pramg6zp.fm. The protonation reactions (eqn (1) and (2)) on edge-sites were:

$$SO^- + H^+ \leftrightarrow SOH,\ KS_1 = [SOH]/([SO^-]\cdot[H^+]) \quad (1)$$

$$SOH + H^+ \leftrightarrow SOH_2^+,\ KS_2 = [SOH_2^+]/([SOH]\cdot[H^+]) \quad (2)$$

The Na^+/H^+ ion-exchange reaction (eqn (3)) on layer-sites was:

$$XNa + H^+ \leftrightarrow XH + Na^+,\ K_{ex} = ([XH][Na^+])/([XNa][H^+]) \quad (3)$$

The sorption reactions (eqn (4)–(10)) were:

$$SO^- + Ra^{2+} \leftrightarrow SORa^+,\ K[1] = [SORa^+]/([SO^-]\cdot[Ra^{2+}]) \quad (4)$$

$$SO^- + RaCO_3 \leftrightarrow SORaCO_3^-,\ K[2] = [SORaCO_3^-]/([SO^-]\cdot[RaCO_3]) \quad (5)$$

$$SO^- + RaPO_4^- \leftrightarrow SORaPO_4^{2-},\ K[3] = [SORaPO_4^{2-}]/([SO^-]\cdot[RaPO_4^-]) \quad (6)$$

$$SO^- + RaHPO_4 \leftrightarrow SORaHPO_4^-,\ K[4] = [SORaHPO_4^-]/([SO^-]\cdot[RaHPO_4]) \quad (7)$$

$$2XH + Ra^{2+} \leftrightarrow X_2Ra + 2H^+,\ K[5] = ([X_2Ra]\cdot[H^+]^2)/([XH]^2\cdot[Ra^{2+}]) \quad (8)$$

$$XH + RaH_2PO_4^+ \leftrightarrow XRaH_2PO_4 + H^+,\ K[6] = ([XRaH_2PO_4]\cdot[H^+])/([XH]\cdot[RaH_2PO_4^+]) \quad (9)$$

$$SO^- + Ra(Ac^-)_2 \leftrightarrow SORa(Ac)_2^-,\ K[7] = [SORa(Ac)_2^-]/([SO^-]\cdot[Ra(Ac)_2]) \quad (10)$$

The balance equations (eqn (11) and (12)) were:

$$\sum SOH = [SO^-] + [SOH_2^+] + [SOH^0] + [SORa^+] + [SORaCO_3^-] + [SORaPO_4^{2-}] + [SORaHPO_4^-] + [SORa(Ac)_2^-] \quad (11)$$

$$\sum X = [XNa] + [XH] + 2\cdot[X_2Ra] + [XRaH_2PO_4] \quad (12)$$

Following input data were also needed: the composition of liquid phase, the phase ratio V/m (L kg^{-1}), the values of stability and dissociation constants of Ra complexes and CO_2 atmospheric pressure (Table 2), protonation constants, ion-exchange constant and total concentration of edge-sites $\sum$SOH and layer-sites $\sum$X (Table 3). All data in the Table 3 were described in detail in publication Kukleva *et al.*[35]

Table 3 Constants describing the surface protolytic properties of *n*HAp, *n*TiO_2 and SPIONs respectively[35,42]

Constant	Units	*n*HAp	*n*TiO_2	*n*Fe_3O_4
Protonation constant – KS_1	[L mol^{-1}]	5.12×10^{11}	2.31×10^6	9.65×10^8
Protonation constant – KS_2	[L mol^{-1}]	1.19×10^5	1.84×10^4	9.13×10^5
Ion-exchange constant – K_{ex}	[—]	3.01×10^6	5.67×10^7	3.60×10^7
Concentration of edge-sites – $\sum$SOH	[mol kg^{-1}]	5.10	0.20	0.05
Concentration of layer-sites – $\sum$X	[mol kg^{-1}]	0.15	0.67	0.09
Specific surface area	[m^2 kg^{-1}]	1.17×10^5	3.30×10^5	1.09×10^5

Table 4 Resulting values of constants K[1–7] of sorption reactions (eqn (4)–(10)) for *n*HAp and $n\mathrm{TiO_2}$

	K[—] ($I = 0$)	
Eqn	*n*HAp	$n\mathrm{TiO_2}$
(4)	$K[1] = 2.44 \times 10^{8}$	$K[1] = 4.13 \times 10^{11}$
(5)	$K[2] = 9.87 \times 10^{4}$	$K[2] = 7.34 \times 10^{11}$
(6)	$K[3] = 3.02 \times 10^{7}$	$K[3] = 1.69 \times 10^{12}$
(7)	$K[4] = 3.79 \times 10^{10}$	$K[4] = 6.16 \times 10^{11}$
(8)	$K[5] = 7.85 \times 10^{-6}$	$K[5] = 7.37 \times 10^{0}$
(9)	$K[6] = 6.60 \times 10^{4}$	$K[6] = 2.34 \times 10^{4}$
(10)	$K[7] = 2.81 \times 10^{8}$	$K[7] = 4.88 \times 10^{11}$
WSOS/DF	0.21	0.18

The results are summarized in Table 4 and Fig. 2 and 3. Experimental data were in a good agreement with calculated values of radium uptake as a function of pH on both edge- and layer-sites (Fig. 2A and 3A). The results of the modelling of the *n*HAp and $n\mathrm{TiO_2}$ labelling with ^{223}Ra support the concept that the radium uptake can be described with the surface complexation model type of CEM and both edge- and layer-sites were involved in sorption mechanism (Fig. 2 and 3). It means, in our opinion, that labelling corresponds better with sorption than with co-precipitation mechanism.

The sorption efficiency (Y%) was calculated based on the equation

$$Y\% = \frac{A_{\mathrm{NP}}}{A_{\mathrm{NP}} + A_{\mathrm{aq}}} \times 100\% \quad (13)$$

where the A_{NP} is the activity of the centrifuged and secondary dispersed nanoparticles [cps], the A_{aq} is the activity of the supernatant [cps]. The A_{NP} and the A_{aq} were measured under the same conditions and no time correction was applied.

The sorption efficiency on *n*HAp was 95 ± 5% in the pH range from 5 to 12 (Fig. 2 and 5). It could be caused by relatively high sorption capacity or high specific surface area of *n*HAp (117 ± 8 $\mathrm{m^2\ g^{-1}}$)[35] and by the composition of used aqueous solution (BRB). Fig. 2 shows that the most important sorption reactions going on edge sites were $RaCO_3$ (eqn (4), minor), $RaPO_4^-$ (eqn (6)) and $RaHPO_4$ (eqn (7)), and on layer-sites were Ra^{2+} (eqn (8)) and $RaH_2PO_4^+$ (eqn (9)). On the base of speciation diagrams (Fig. 1), the greater role of PO_4^{3-}, CO_3^{2-} and CH_3COO^- ligands were expected, but this supposition especially in a case of acetic anion was not confirmed. However, the role of HPO_4^{2-} seems to be underestimated.

In the case of $n\mathrm{TiO_2}$ sorption efficiency was about 100% in pH range from 3 to 12 and decreased to 75% at lower pH values (Fig. 3 and 5), which could be also caused by high sorption

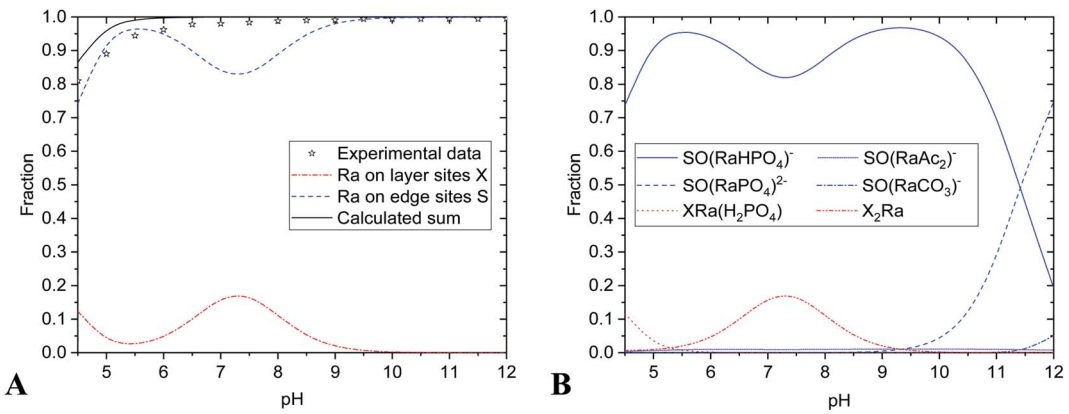

Fig. 2 Sorption on *n*HAp: (A) ^{223}Ra uptake *vs.* pH; (B) uptake of given species *vs.* pH.

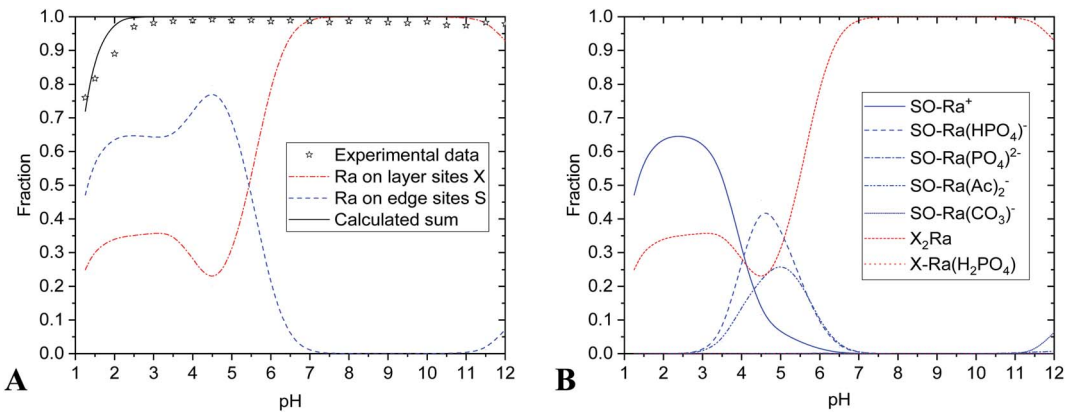

Fig. 3 Sorption on $n\mathrm{TiO_2}$: (A) ^{223}Ra uptake *vs.* pH; (B) uptake of given species *vs.* pH.

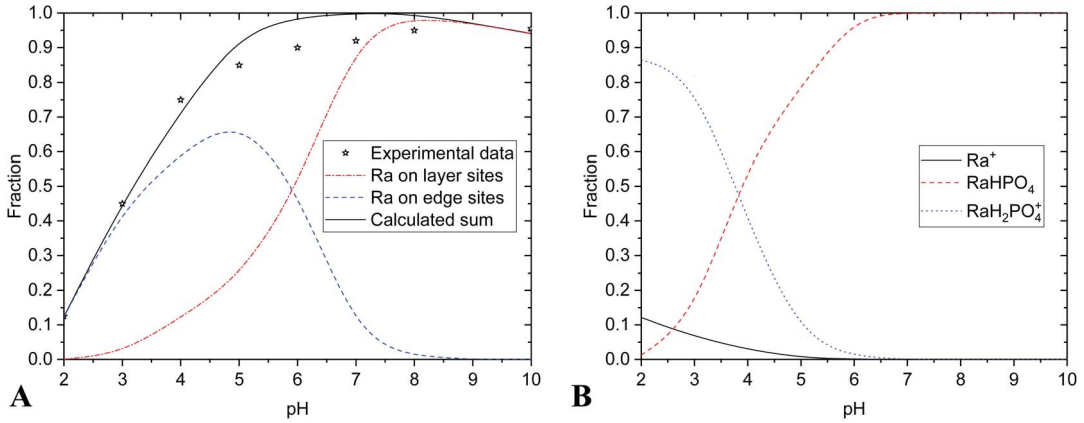

Fig. 4 Sorption on SPIONs: (A) ^{223}Ra uptake *vs.* pH; (B) uptake of given species *vs.* pH.

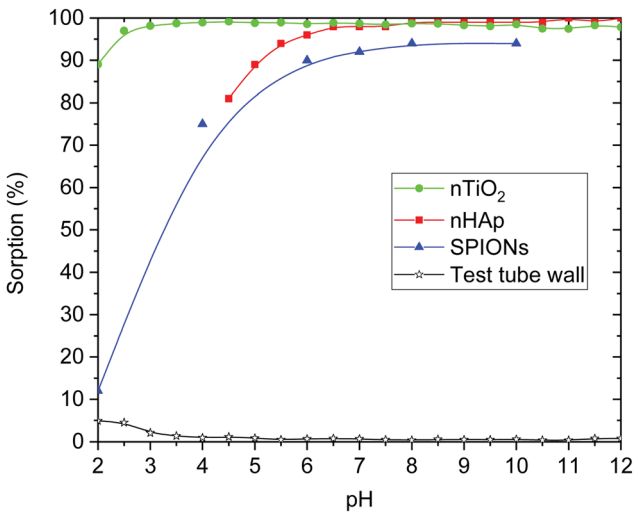

Fig. 5 Dependence of sorption yield on pH value for *n*HAp, *n*TiO_2, SPIONs and plastic test tube wall.

capacity or high specific surface area (330 ± 10 m^2 g^{-1})[35] of *n*TiO_2, and also due to the composition of aqueous phase. The main role in sorption reactions on layer-sites played Ra^{2+} itself (eqn (8) and Fig. 3). On edge-sites the most important species seems to be Ra^{2+} (eqn (4)), $RaCO_3$ (eqn (5)), $RaHPO_4$ (eqn (7)) and $Ra(Ac^-)_2$ (eqn (10)) (Fig. 4). On the base of speciation diagrams, the greater role of PO_4^{3-} (Fig. 1A) and CH_3COO^- (Fig. 1B) ligands were expected, however this expectation were not verified. One of the most interesting result is that surface complexation model type of CEM is suitable as a describing model of studied *n*TiO_2 radium uptake, as well as of *n*HAp.

Certainly, the question considering presence of atmospheric CO_2 also needs to be taken into account. Relatively high concentrations of carbonates in samples with pH greater than 8–9 could affect the results, therefore, it might be better to use inert atmosphere for clearer experiments. In spite of this, the CO_2 and HCO_3^- were included in calculations.

Radium sorption properties of *n*HAp and *n*TiO_2 were compared also with SPIONs (Fig. 4 and 5).[42] From comparison, it is evident that all three materials have relatively high sorption affinity to $Ra^{(II)}$ under the studied conditions. It is necessary to keep in mind that low initial radium concentrations were used (approx. 2 kBq, 5×10^{-12} M). Although there were some differences in the values of parameters of edge-sites (KS_1, KS_2, $\sum$SOH), of layer-sites (K_{ex}, $\sum$X) and of the specific surface area, sorption yields for all three materials were high. Additional

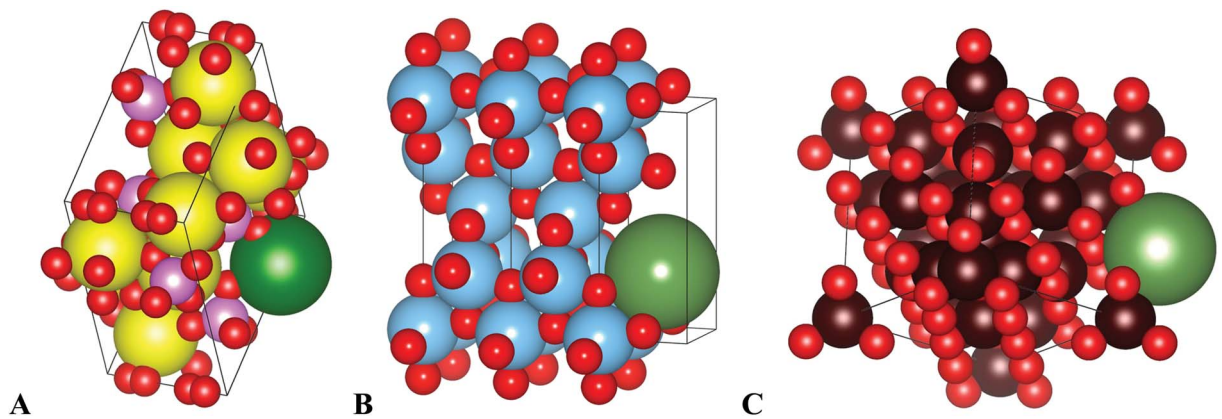

Fig. 6 Schematical drawing of radium uptake in (A) *n*HAp, (B) *n*TiO_2, (C) SPIONs. Yellow – calcium, blue – titanium, dark red – iron, green – radium, red – oxygen, pink – phosphorus. Images were created in Vesta software.[43]

distinction of *n*HAp towards $n\text{TiO}_2$ and SPIONs was its lower chemical stability in acidic aqueous solutions. Regarding its possible application *in vivo*, it should not play any significant role.

The values of *n*HAp's and $n\text{TiO}_2$'s $K\text{S}_1$ (equilibrium constant of reaction eqn (1)) indicated the relatively greater shift of *n*HAp's protonation reaction (eqn (1)) to the right in comparison to the $n\text{TiO}_2$. In relation to $K\text{S}_1$ values, the deprotonated species SO^- did not exist in pH lower than 6 in the case of *n*HAp and lower than 5 for $n\text{TiO}_2$.[35] This fact played a certain role in ion-exchange reactions (eqn (3)) and surface complexation reactions (eqn (4)–(7) and (10)).

Comparing all three materials, it could be said that all of them have comparable properties in the context of Ra sorption (Fig. 5 and 6). Hydroxyapatite nanoparticles as well as SPIONs showed high yields of ^{223}Ra uptake at pH over 6. In the case of *n*HAp, it could be due to low chemical stability of nanomaterial at lower pH. In the case of SPIONs, it is probably caused by presented species (SPIONs labelling was performed in PBS, where the main component is phosphate and at pH lower than 6 it was presented in the form of H_3PO_4 and H_2PO_4^- (Fig. 4)).[42] Chemically stable $n\text{TiO}_2$ has shown very high sorption yields at pH 2.5 and higher. It is also important to notice, that sorption of all presented radium species on plastic was negligible (Fig. 5).

Despite CO_2 presence interfere and tangle modelling, it did not affect experimental the sorption results. This can be extremely beneficial for easier experimental setup, where necessary requirements could be lower.

Furthermore, another interesting result was that there was a good evidence for the modelling of radium uptake (labelling, sorption) on nanoparticles of *n*HAp, $n\text{TiO}_2$ and SPIONs by means of the surface complexation model type of CEM, in spite of the fact, that studied materials were not similar.

Conclusions

Studied materials *n*HAp and $n\text{TiO}_2$ had shown relatively high sorption affinity to $\text{Ra}^{(\text{II})}$ under the studied conditions and the radiolabelling yields were over 95% in a wide pH range. Based on the calculations and modelling it was found, that the main role in sorption in the case of *n*HAp played RaCO_3, RaPO_4^-, RaHPO_4, Ra^{2+} and $\text{RaH}_2\text{PO}_4^+$. In the case of $n\text{TiO}_2$ the main role in sorption reactions played Ra^{2+} itself, RaCO_3, RaHPO_4 and $\text{Ra}(\text{Ac}^-)_2$. Furthermore, it was found, that presence of CO_2 did not interfere high sorption yields, what could be important to take into account for further experiments.

This paper shows possibility to use *n*HAp and $n\text{TiO}_2$ nanoparticles as a useful vehicle for ^{223}Ra delivery for targeted alpha therapy. So, it could be concluded, that *n*HAp and $n\text{TiO}_2$ are suitable nanomaterials for medicinal usage due to high sorption properties in a pH range required for medicine, radiation stability and biocompatibility. Another important benefit is labelling procedure simplicity, where radium chloride in a liquid form is mixed with ready-made particles under laboratory temperature without any inert atmosphere. Obviously, this study is preliminary and further investigations of labelling kinetics and *in vitro* stability in biologically relevant media are necessary.

Conflicts of interest

There are no conflicts to declare.

Acknowledgements

This work was supported by the grants of NV16-30544A (Czech Health Research Council), CZ.02.1.01/0.0/0.0/15_003/0000464 (EU and the Ministry of Education, Youth and Sports of the Czech Republic), and SGS19/194/OHK4/3T/14 (Czech Technical University in Prague).

References

1 U.S. National Library of Medicine, *Toxicology Data Network*, November 2019, Available on: https://toxnet.nlm.nih.gov/newtoxnet/index.html.
2 M. P. Ferraz, F. J. Monteiro and C. M. Manuel, *J. Appl. Biomater. Funct. Mater.*, 2004, **2**(2), 74–80.
3 S. Koutsopoulos, *J. Biomed. Mater. Res.*, 2002, **62**(4), 600–612.
4 W. Kreyling, U. Holzwarth, N. Haberl, J. Kozempel, S. Hirn, A. Wenk, C. Schleh, M. Schäffler, *et al.*, *Nanotoxicology*, 2017, **11**(4), 434–442.
5 M. Malekshahi Byranvand, A. Nemati Kharat, L. Fatholahi and Z. Malekshahi Beiranvand, *J. Nanostruct.*, 2013, **3**, 1–9.
6 S. Mital Gupta and M. Tripathi, *Cent. Eur. J. Chem.*, 2012, **10**(2), 279–294.
7 A. Salvador, M. C. Pascual-Martí, J. R. Adell, A. Requeni and J. G. March, *J. Pharm. Biomed. Anal.*, 2000, **22**(2), 301–306.
8 Y. Matsumura and H. Maeda, *Cancer Res.*, 1986, **46**(12), 6387–6392.
9 H. Maeda, K. Tsukigawa and J. Fang, *Microcirculation*, 2016, **23**(3), 173–182.
10 J. A. Nagy, S.-H. Chang, A. M. Dvorak and H. F. Dvorak, *Br. J. Cancer*, 2009, **100**(6), 865–869.
11 K. Van Butsele, R. Jérôme and C. Jérôme, *Polymer*, 2007, **48**(26), 7431–7443.
12 J. Kozempel, M. Vlk, E. Málková, A. Bajzíková, J. Bárta, R. Santos-Oliveira and A. Malta Rossi, *J. Radioanal. Nucl. Chem.*, 2014, **34**(1), 443–447.
13 L. D. Esposti, A. Tampieri and M. Iafisco, in *Nanotechnologies in Preventive and Regenerative Medicine*, ed. V. Uskokovic, Elsevier, New York, 2017, ch. 6.3, pp. 465–486.
14 M. Sakmar, M. Vlk, P. Suchankova, E. Kukleva, J. Kozempel, M. Hruby and V. Lobaz, *presented in part at 13th international symposium on the synthesis and application of isotopically labelled compounds*, Prague, June 2018.
15 P. Micolova, E. Kukleva, P. Nykl, M. Sakmar, M. Vlk, L. Nespesna and J. Kozempel, *J. Labelled Compd. Radiopharm.*, 2017, **60**(S1), S283.
16 S. Chakraborty, K. V. Vimalnath, A. Rajeswari, H. D. Sarma, A. Shinto, E. R. Radhakrishnan and A. Dash, *J. Radioanal. Nucl. Chem.*, 2017, **302**(2), 875–881.

17 G. Sgouros, A. M. Ballangrud, J. G. Jurcic, M. R. McDevitt, J. L. Humm, E. Y. Erdi, B. M. Mehta, R. D. Finn, S. M. Larson and D. A. Scheinberg, *J. Nucl. Med.*, 1999, **40**(1), 1935–1946.
18 W. Zhou and J. Zheng, *Adv. Mater. Res.*, 2012, **503/504**, 688–691.
19 J. Xie, S. Lee and X. Chen, *Adv. Drug Delivery Rev.*, 2010, **62**(11), 1064–1079.
20 C. Apostolidis, R. Molinet, J. McGinley, K. Abbas, J. Möllenbeck and A. Morgenstern, *Appl. Radiat. Isot.*, 2005, **62**(3), 383–387.
21 S. Handley-Sidhu, T. K. Mullan, Q. Grail, M. Albadarneh, T. Ohnuki and L. E. Macaskie, *Sci. Rep.*, 2016, **6**(1), 1–8.
22 W. G. Kreyling, U. Holzwarth, C. Schleh, J. Kozempel, A. Wenk, N. Haberl, S. Hirn, M. Schäffler, J. Lipka, M. Semmler-Behnke and N. Gibson, *Nanotoxicology*, 2017, **11**(4), 443–453.
23 G. Xie, C. Wang, J. Sun and G. Zhong, *Toxicol. Lett.*, 2011, **205**(1), 55–61.
24 E. Cedrowska, M. Pruszynski, A. Majkowska-Pilip, S. Meczyńska-Wielgosz, F. Bruchertseifer, A. Morgenstern and A. Bilewicz, *J. Nanopart. Res.*, 2018, **20**, 83, DOI: 10.1007/s11051-018-4181-y.
25 S. Bassot, C. Mallet and D. Stammose, *MRS Online Proc. Libr.*, 2000, **663**, 1081.
26 M. Sajih, N. D. Bryan, F. R. Livens, D. J. Vaughan, M. Descostes, V. Phrommavanh, J. Nos and K. Morris, *Geochim. Cosmochim. Acta*, 2014, **146**, 150–163.
27 J. M. Zachara, C. E. Cowan and C. T. Resch, *Geochim. Cosmochim. Acta*, 1991, **55**(6), 1549–1562.
28 European Medicines Agency, *Xofigo*, June 2019, Available on: https://www.ema.europa.eu/en/medicines/human/EPAR/xofigo.
29 S. Nilsson, P. Srang, A. K. Aksnes, L. Franzèn, P. Olivier, A. Pecking, J. Staffurth, S. Vasanthan, C. Andersson and Ø. S. Bruland, *Eur. J. Cancer*, 2012, **48**(5), 678–686.
30 S. Mirzadeh, *Appl. Radiat. Isot.*, 1998, **49**(4), 345–349.
31 O. Mokhodoeva, L. Guseva and N. Dogadkin, *J. Radioanal. Nucl. Chem.*, 2014, **304**(1), 449–453.
32 E. Kukleva, J. Kozempel, M. Vlk, P. Micolova and D. Vopalka, *J. Radioanal. Nucl. Chem.*, 2014, **304**(1), 263–266.
33 L. I. Guseva, G. S. Tikhomirova and N. N. Dogadkin, *Radiochemistry*, 2004, **46**(1), 58–62.
34 WWW, *Table of radioactive isotopes: nuclide search*, June 2019, Available on: http://nucleardata.nuclear.lu.se/toi/nucSearch.asp.
35 E. Kukleva, P. Suchankova, K. Stamberg, M. Vlk, M. Slouf and J. Kozempel, *RSC Adv.*, 2019, **9**, 21989–21995.
36 H. Filipská and K. Štamberg, *Acta Polytech.*, 2005, **45**(5), 11–18.
37 H. Wanner, Y. Albinsson, O. Karnland, E. Wieland, P. Wersin and L. Charlet, *Radiochim. Acta*, 1994, **66**(67), 157–162.
38 ZZ HATCHES-20, *Database for radiochemical modelling*, May 2019, Available on: https://www.oecd-nea.org/tools/abstract/detail/nea-1210.
39 L. Dvořák, T. Ledvinka and M. Sobotka, *FAMULUS 3.1*, 1991, Custom made software, Prague, Czech Republic.
40 A. L. Herbelin and J. C. Westall, *FITEQL 3.2, Custom made software*. Department of Chemistry, Oregon State University, Corvallis, Oregon, USA, 1996.
41 ThermoChimie, *Thermodynamic database*, August 2019, Available on: https://www.thermochimie-tdb.com.
42 O. Mokhodoeva, M. Vlk, E. Málková, E. Kukleva, P. Mičolová, K. Štamberg, M. Šlouf, R. Dzhenloda and J. Kozempel, *J. Nanopart. Res.*, 2016, **18**(10), 1–12.
43 K. Momma, August 2019, Available on: https://jp-minerals.org/vesta/en/.

